Ultrasonics Sonochemistry 90 (2022) 106209

Contents lists available at ScienceDirect

Ultrasonics Sonochemistry

journal homepage: www.elsevier.com/locate/ultson

Free surface entrainment of oxide particles and their role in ultrasonic treatment performance of aluminum alloys

Jincheng Sun [a,*], Kennosuke Higashi [b], Sergey Romankov [b], Takuya Yamamoto [a,b], Sergey Komarov [a,b]

[a] Graduate School of Environmental Studies, Tohoku University, 6-6-02 Aza Aoba, Aramaki, Aoba-ku, Sendai, Miyagi 980-8579, Japan
[b] Department of Metallurgy, Materials Science and Materials Processing, Graduate School of Engineering, Tohoku University, 6-6-02 Aza-Aoba, Aramaki, Aoba-ku, Sendai 980-8579, Japan

ARTICLE INFO

Keywords:
Molten aluminum
Ultrasonic treatment
Melt free surface
Particles entrainment
Primary Al_3Zr compound

ABSTRACT

Although the ultrasonic treatment of molten aluminum has been studied for long period, there is still much to be revealed for this process. Many studies have focused on the investigation of acoustic cavitation and streaming under the horn tip and their effects on the treatment efficiency. However, to the best of our knowledge, no attempt has been done to explain phenomena occurring near or on the melt free surface. Thus, the goal of this study is to investigate phenomena occurring at the free surface during ultrasound irradiation and clarify their possible influence on the ultrasound treatment performance. The results of high temperature and water model experiments reveal that ultrasound irradiation significantly promotes the formation of alumina particles on the melt free surface around sonotrode, and part of these particles can be entrained into aluminum melts. Furthermore, TEM observation results suggested that the entrained alumina inclusions can serve as nucleation sites for the primary Al_3Zr compounds. Most importantly, the oxidation and entrainment of particles from free surface are likely to be controllable by the immersion depth of sonotrode into molten aluminum.

1. Introduction

The first pioneering works on the treatment of liquid metal by ultrasound (hereinafter referred to as UST) can date back to the 1930s. [1] There are two important phenomena, namely cavitation and acoustic streaming, which occur when ultrasound vibrations are introduced in a liquid under appropriate conditions. Specifically, the vibration amplitude should exceed a threshold value for a stable cavitation field to be generated. This threshold value depends on such factors as type of liquid, content of gas and solid impurities in liquid. For instance, it was found that the peak-to-peak threshold amplitudes in tap water and commercially pure aluminum melt were 4–5 μm and 10–11 μm respectively at a frequency of 20 kHz. [2,3] Another phenomenon is acoustic streaming which is initiated in the cavitation zone beneath sonotrode tip due to an attenuation of the ultrasound energy there. [4].

The utilization of cavitation and acoustic streaming for improving the solidification structure of aluminum alloys has been extensively investigated in the past[5–11]. It has been recognized that these two phenomena can play different roles during solidification process depending on the temperature of ultrasound irradiation. When UST is performed at a temperature near or lower than T_L (hereinafter T_L referred as to liquidus temperature), a number of mechanisms are responsible for the UST effects. These mechanisms include mainly fragmentation and modification of primary solidifying phases as well as improvement in fluidity of melt in the mushy zone. There is a large volume of literature on this topic including books [12–14] and papers [16–18]. Their main results can be briefly summarized as follows. At temperatures lower than T_L, cavitation bubbles, when collapse near primary solidified crystals, can cause their mechanical fragmentation [15–18], which is considered to be the main mechanism of microstructure refinement at $T < T_L$. In addition, cavitation-induced microstreaming influences the mass transfer between the melt and growing crystals, and this is capable of changing the crystal shape [16]. This effect is commonly called modification. Besides, when ultrasonic vibrations are introduced into the sump of a DC caster, the acoustic streaming and turbulent oscillations alter characteristics of the mushy zone [19–21] that can be effective in preventing hot-tearing in high-speed casting of aluminum alloys [22] and in improving the quality of

* Corresponding author.
E-mail address: un.jincheng.q8@dc.tohoku.ac.jp (J. Sun).

https://doi.org/10.1016/j.ultsonch.2022.106209
Received 29 July 2022; Received in revised form 3 October 2022; Accepted 5 October 2022
Available online 25 October 2022

billet surface [18].

At temperatures higher than T_L, the main role of ultrasound treatment is dispersion and activation of refiner particles when they are introduced to the melt. Typical examples of such particles are AlP, TiB_2 and TiC which promote nucleation of primary silicon (AlP) or aluminum (TiB_2, TiC) grains. It has been recognized that this effect is due to the low lattice misfits between the crystal structure of solidifying phases and refiners. For example, in casting of Al-Si hypereutectic alloys [23,24] particles of primary silicon can be significantly refined by ultrasound vibrations introduced in the melt. This refinement effect was found to result from the dispersion of AlP particles in cavitation zone that enhances the particle nucleation potency [25]. Besides, some primary intermetallic compounds of Al-Ti or Al-Zr-Ti systems can also serve as nucleation sites for aluminum grains. For example, Wang et al. [11] investigated the effect of ultrasonic melt treatment on the refinement of primary Al_3Ti intermetallic in an Al–0.4Ti alloy, and found that cavitation-enhanced nucleation via improved wetting of native particles plays the dominant role in refinement when the UST is applied in the fully liquid state. Atamanenko et al. [19] revealed that the grain size and morphology of pure aluminum can be significantly refined with 10 s UST in the liquid state.

At the same time, results of some recent studies reveal that the refinement and modification effect of UST at $T > T_L$ can be achieved even when no refiners are added. For examples, Eskin [7] reported that oxide particles in aluminum melt can promote the nucleation of cavitation bubbles during ultrasound irradiation, and these bubbles then can enhance the melt degassing and influence the solidification phenomena. During the casting process of aluminum alloys, it is difficult to avoid entering oxide particles in the melt. Particularly such oxides as alumina and its spinel are often entrained into molten aluminum. Obviously, the main source of such particles is oxidation of aluminum and alloying elements by atmospheric moisture and oxygen. According to recent studies, fine oxide particles can serve as nuclei for some intermetallic compounds and α-Al grains. The finding provides a plausible explanation of why the refinement effect of ultrasound is sometimes observed even after the treatment at temperatures higher than T_L without refiner addition. For example, Wang et al. [15] clarified the refining mechanism of primary Al_3Ti compounds during an ultrasonic treatment at a temperature at which the compounds still do not exist in the melt. They used an edge-to-edge matching model and experimental determination of crystallographic orientation relationships between the α-Al_2O_3 and primary Al_3Ti particles and the results confirmed high potency of α-Al_2O_3 particles as nucleation sites for the Al_3Ti compounds. Sreekumar et al. [26] suggested that the calculated lattice misfit of solid aluminum at 660^{O}C with γ-Al_2O_3 and α-Al_2O_3 is 3.38 % and −0.48 % respectively. These results indicate that these oxides can be highly potent for nucleation of α-Al grains. Mechanisms of enhanced heterogeneous nucleation during solidification in binary Al–Mg alloys were investigated by Li et al. [27] They found that one of them can be attributed to $MgAl_2O_4$ particles acting as potent sites for nucleation of α-Al grains with a lattice misfit of 1.4 %. A well-defined orientation relationship between α-Al and $MgAl_2O_4$ was also observed and identified [28] to be: 8.5 degrees (-1 1–1)α-Al//(2–2 2)$MgAl_2O_4$, and [−110]α-Al//[−110] $MgAl_2O_4$, and it was also demonstrated that the native $MgAl_2O_4$ particles are sufficient to enhance the heterogeneous nucleation of α-Al. The effect of melt conditioning on segregation of solute elements and nucleation of aluminum grains in a twin roll cast aluminum alloy was examined by Kim [29]. The results suggested that MgO particles can act as a substrate for nucleation of aluminum however this. Specifically, oxide particles of about 1 to 5 μm in size possess a higher potency to nucleate aluminum grains under lower undercooling of heterogeneous nucleation onset. On the other hand, finer oxide particles with the size of about 100 to 200 nm requiring larger undercooling degree were found to be pushed towards the grain boundaries during solidification and could not serve as nucleation sites.

Thus, the results of the above-mentioned studies suggest that non-metallic inclusions, particularly alumina, which inevitably enter the aluminum melt, may additionally contribute to the improvement of solidification structure. This effect should be especially significant when the nucleation potency of such inclusions is enhanced by ultrasound.

Recent findings, however, suggest that the role of ultrasound vibrations may be not limited to the dispersion and activation of inclusion particles that are already present in melt. Another useful effect is that ultrasound vibrations can promote formation of oxide particles and their entrainment in the molten bath. It is a well-known fact that the surface of aluminum melt is covered with thin oxide film due to extremely high affinity of aluminum to oxygen. Such films with nanometer thickness [30] can be fragmented into tiny particles which can be entrained into the melt. Nevertheless, to the best of our knowledge, no study has been done to investigate these phenomena under application of ultrasound vibrations.

Entrainment of particles from the free surface, however, has been a subject of considerable interest in other fields such as mechanical stirring and agitation. For example, Komarov et al. [31] investigated incorporation of fine particles into liquid from the free surface of a large-scale swirling vortex created around the axis of a rotary impeller in a cylindrical vessel. Two feasible mechanisms for particle penetration behavior were proposed. The first one is an oscillating motion of the vortex free surface causing particles to enter into the liquid due to inertial force. Then, such particles could be easily entrained into the liquid bulk due to turbulent eddies. The second mechanism is related to capillary phenomena which force the liquid to rise up through narrow capillaries between the particles. Kang et al. [32] used discrete element model coupled with volume of fluid method (DEM-VOF) to simulate the entrainment of floating particles from the free surface into a turbulent flow in stirred vessels. The results revealed that the entrainment process can be divided into three stages, namely pull-down, dispersion and cycle stage, sequentially. It was found that particles incorporate from the free surface into the liquid bulk due to an increase of pulling force in the vertical direction. As mentioned above, introduction of ultrasound vibrations in the melt is responsible for such phenomena as cavitation, acoustic flow and turbulence and, hence, can influence the behavior of particles on the free surface including their formation and entrainment in the melt bulk.

Thus, the main goal of present study is to examine whether ultrasound vibrations influence the formation of oxide particles at the free surface of molten aluminum and to investigate the behavior of such particles, particularly their entrainment into the melt bulk. The experiments include two parts, namely high temperature experiments using pure aluminum or an Al-Zr alloy, and water model experiments. In high temperature experiments, particles, collected after 2-hour ultrasonic treatment, were analyzed for phase composition and size distribution. Then, non-metallic inclusions in aluminum ingots were investigated with PoDFA (Porous Disk Filtration Apparatus) method to confirm the presence of alumina particles in the melt and to examine their characteristics Possible mechanisms of particle entrainment were clarified by water model experiments using a high-speed video camera. The results obtained were explained taking into account cavitation-related phenomena and downward acoustic flows. Besides, SEM and TEM observations were performed to examine the probability for the particles to serve as nucleation sites for the deposition of Al-Zr primary compounds.

2. Experimental

2.1. High temperature experiments

Approximately 2 kg of commercially pure aluminium (99.9 %) was charged into a CP crucible of 122 (O.D.) × 98 (I.D.) × 200 (H) mm in size. Aluminum contained iron and silicon as impurities in concentration of 0.06 % and 0.04 %, respectively. In experiments with Al-0.4 %Zr, 190 g of Al-5 %Zr master alloy was charged into the crucible together with aluminum.

The charge was then melted and heated up to 1173 K using an electrical resistance furnace placed on an elevating platform as shown in Fig. 1 (a). The melt was held for 2 h before treatment. The ultrasonic treatment was performed inside the furnace at a constant temperature of 1023 and 1083 K for pure Al and Al-0.4 %Zr alloy, respectively. A K-type thermocouple was used to monitor the melt temperature. According to the Al-Zr phase diagram shown in Fig. 2, the liquidus temperature (T_L) of Al-0.4 %Zr alloy was approximately 1073 K. Therefore, UST was performed above T_L. More details can be found in our earlier publication [33].

The ultrasound equipment was basically the same as that used in the above-mentioned publication. The only difference is that in the present study UST was done inside the furnace. Therefore, before UST, the distance between the sonotrode tip and the melt surface was gradually reduced for the sonotrode preheating for 30 min. The sonotrode was made of Si_3N_4-based ceramics. It is worth noting that the sonotrode has extremely high erosion resistance. [34] Therefore contamination of melt by Si_3N_4 particles during 2-hour treatment can be neglected.

After that, the sonotrode was immersed in the melt as shown in Fig. 1 (d) to start UST. Temperature range and duration of ultrasound treatment, vibration amplitude of sonotrode tip and melt pouring temperature are summarized in Table 1. The melt temperature during the ultrasonic treatment process was controlled by changing the furnace output power. Finally, the melt was poured into a steel boat mold with a length and width of 250 and 35 mm, respectively. The cooling rate was determined from preliminary measurements using a fast response K-type thermocouple and a datalogger with a sampling rate of 1 ms/s. At the ingot location, from where all samples were cut, the cooling rate was 20 K/*sec*.

Observations during the UST process revealed a formation of tiny black particles on the surface of pure Al melt around the sonotrode. The particles were collected before casting and then analyzed for the phase composition by XRD. (SmartLab 9kw, Rigaku) Additionally, the particle size distribution was analysed by a particle size analyzer (Seishin, LMS-2000e, Japan). For the sake of comparison, experiments without UST were also carried out under the same conditions. The ingots obtained in the experiments with and without UST were then used to analyze non-metallic inclusions, particularly alumina particles, by PoDFA technique (Porous Disk Filtration Apparatus). This technique is the commonly used industry standard for assessing the cleanliness of aluminum melts. More details about the principle of PoDFA analysis can be found in the relevant literature, for example in [35]. In the present PoDFA test, approximately 2 kg of aluminum melt was passed through a ceramic filter with diameter of pores 77 μm. Then, following the standard procedure, a part of filters with the solidified aluminum was used to prepare samples for observation and analysis of particles trapped in the filter pores. Appearance of such a sample is illustrated in Fig. 3, and the filter part is marked by the red dotted square. The sample

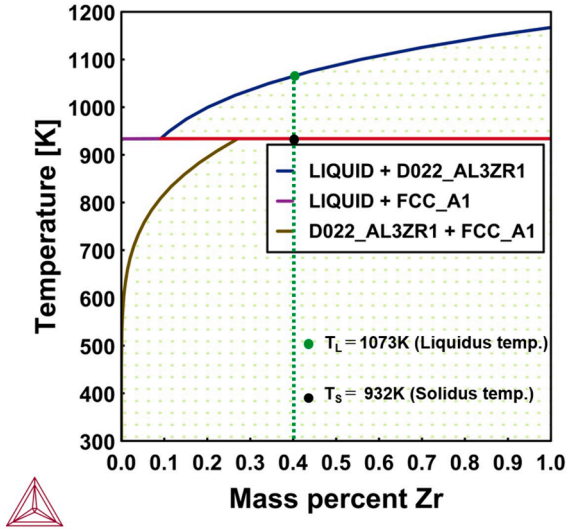

Fig. 2. Al-Zr phase diagram.

Table 1
Ultrasonic treatment and casting conditions for pure Al and Al-0.4%Zr alloy.

UST				
Material	Temperature range (K)	Amplitude (μm, p-p)	Time (h)	Pouring temperature (K)
Pure Al	1023 ± 10	58	2	963 ± 2
Pure Al	–	–	–	963 ± 2
Al-0.4 % Zr	1083 ± 10	58	2	1023 ± 2

microstructure was observed by an optical microscope (Olympus, BX53M, Japan) and field-emission scanning electron microscope (FE-SEM; JEOL JSM-6500F) with emphasis on the two areas: the interface between filter and solidified Al as well as inside the filter pores filled by Al. More details can be found in the following section.

After experiments using Al-0.4 %Zr alloy, samples of 10×10×5 mm^3 in size were cut out from the ingot and then prepared for analysis using standard metallographic techniques. The microstructure was observed by a field-emission scanning electron microscope (FE-SEM; JEOL JSM-6500F) and Transmission electron microscope (TEM; JEM-ARM200F (JEOL)) with 200 kV accelerating voltage.

2.2. Water model experiments

Fig. 4 is a schematic diagram of setup used for water model

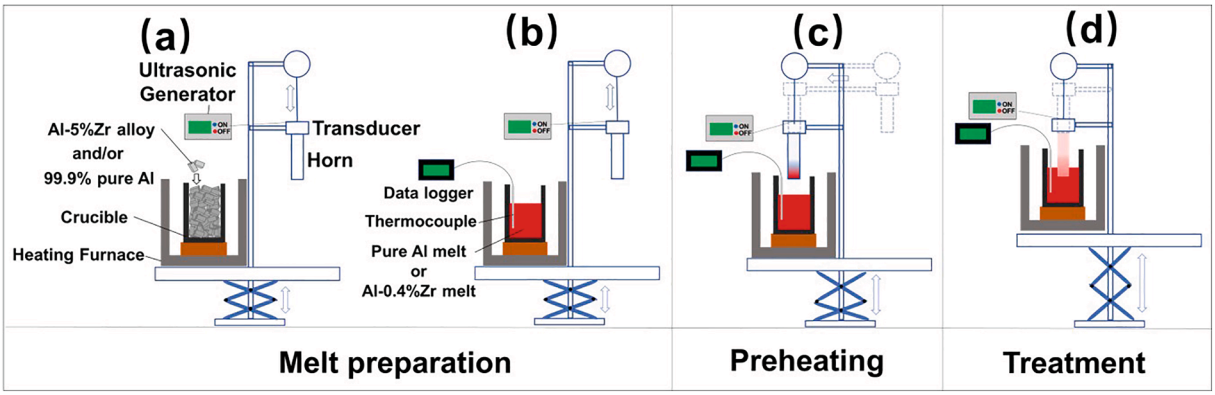

Fig. 1. Schematic representation of experimental setup and procedure for high temperature experiments.

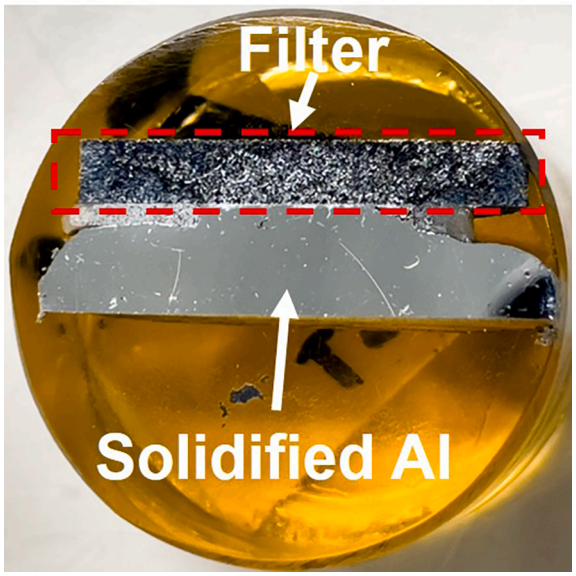

Fig. 3. A photograph of a sample after PoDFA analysis.

experiments. As mentioned above, the main goal of these experiments was to directly observe particles entrainment phenomena from the free surface of a water bath during ultrasound irradiation. For this purpose, a high-speed camera (FASTCAM Nova S12, Photron) equipped with a lense (LEICA Z16 APO, Leica) was installed in the opposite side of a high intensity LED light device (UFLS-751-08 W-UT, U-Technology). As indicated in Fig. 4, an acrylic vessel with dimension of 190 (L) × 30 (W) × 210 (H) mm was used. A special plate-shaped ultrasound sonotrode was designed for these experiments. The sonotrode tip had width and thickness of 20 and 6 mm, respectively. 20-kHz ultrasonic vibrations were introduced through this sonotrode in the water bath at an amplitude of 52 μm (peak-to-peak). The amplitude was measured using a high-speed laser displacement sensor (LK-G5000, Keyence, Japan) in the air environment. Table 2 present the properties of polymethyl methacrylate particles used in these experiments as model particles.

The experiments were carried out according to the following procedure:

*The vessel was filled by water and placed between the above-mentioned video camera and light source.

*The sonotrode was immersed into water to a depth of around 10 mm.

*The particles were added to the water surface in the vicinity of sonotrode.

*The high-speed camera and light were switched on to start recording at a frame rate of 500 fps and a shutter speed of 1/1000 *sec*.

*The ultrasound irradiation into water was started.

During ultrasound irradiation process, the phenomena occurring near the sonotrode were recorded by the video camera. The size of video images was approximately 550 μm in width and 280 μm in height. The pixel resolution of image was 256×128. Thus, dimension of each pixel was around 2 μm. A number of snapshots was taken to explain particles entrainment phenomena from the water free surface and the corresponding video documents can be found in supplementary materials.

3. Results

3.1. Formation of alumina particles on the melt surface

Fig. 5 shows the black particles on the melt surface after 2-hours UST. As it can be seen from Fig. 5(a), the Al melt surface is free of black parties before UST. However, a large number of black particles are clearly seen around the sonotrode as indicated in Fig. 5(b). Fig. 6(a) shows their XRD spectrum. It is seen that is the particles are composed of aluminum and its oxide including α-Al_2O_3 and γ-Al_2O_3. As for the first oxide, a number

Table 2
Properties of particles used in the water model experiments.

Material	Density, ρ_p	Wetting Angle, θ	Diameter, d_p
	kg/m^3	deg.	μm
PMMA	1200	76	60

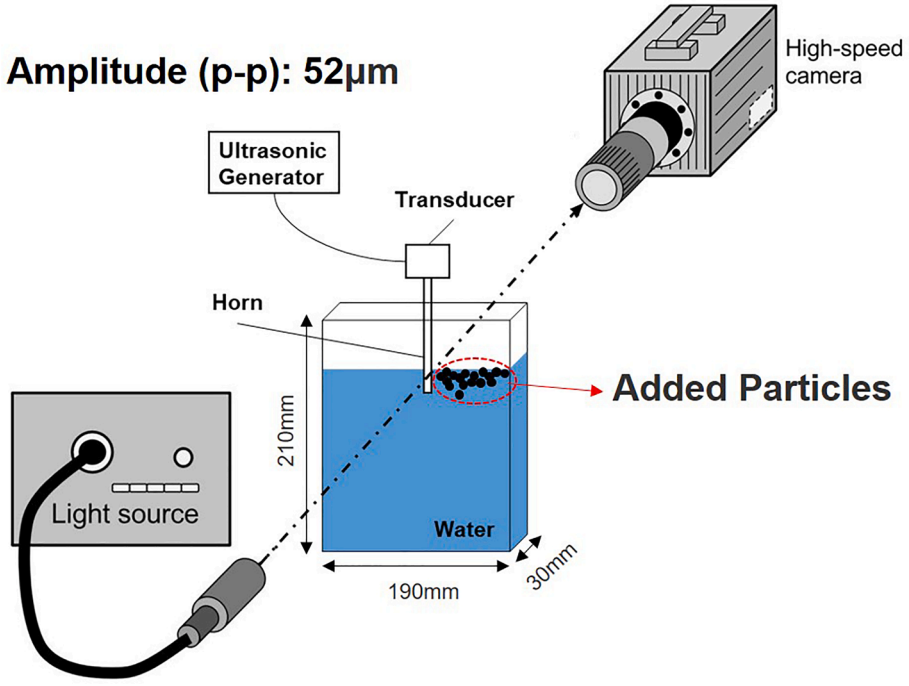

Fig. 4. A schematic diagram of setup for water model equipment.

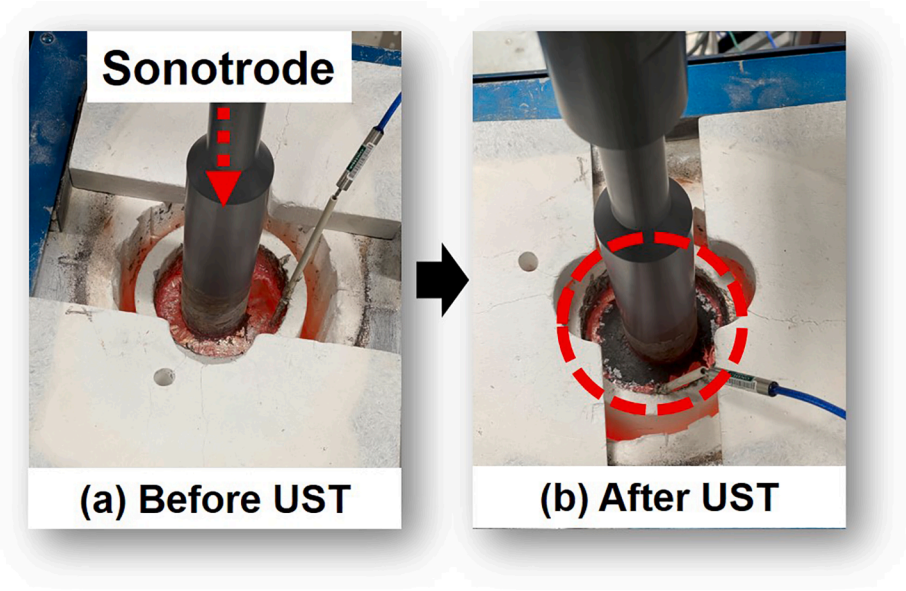

Fig. 5. A photograph of the Al melt surface before (a) and after (b) UST.

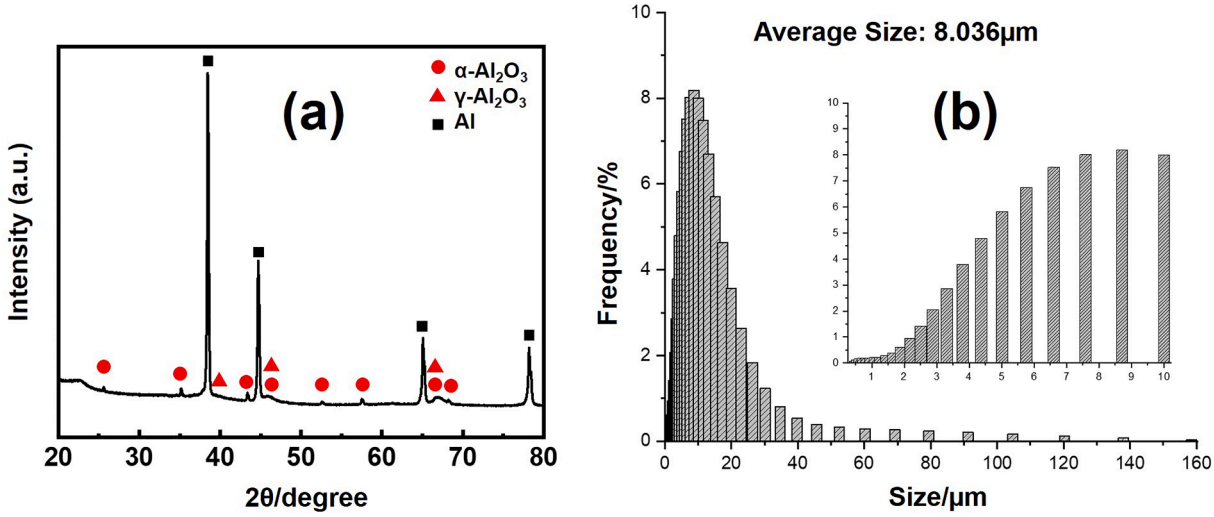

Fig. 6. XRD results for black particles collected from the melt surface after 2 h UST: (a); and their size distribution: (b).

of small peaks were detected. On the other hand, only two γ-Al_2O_3 peaks were observed in the spectrum presumably because the other peaks were overlapped with the α-Al_2O_3 peaks. The appearance of strong Al peaks because some amount of aluminum might enter the sample during collecting process. Another reason might be that some relatively large particles could be composed of aluminum core and alumina shell. Fig. 6 (b) presents the size distribution of collected particles. It is seen that the distribution follows a logarithmic normal probability distribution with the average size of 8.036 μm. The formation process of these particles will be discussed in the next section.

3.2. PoDFA analysis results

It should be noted that the PoDFA analysis provides both qualitative information on the nature of inclusions and quantitative information on the inclusion quantity. Particularly, one of the characteristics which can be evaluated from the PoDFA analysis, is the number of inclusions per unit surface area of filter. Fig. 7 presents two optical microscopy photographs of filter surface when samples with UST (a) and without UST (b) were used for filtration. A greater number of particles can be seen after 2-hour UST as compared to the case without UST. In addition, quantitative estimates were made based on the total surface area of filter occupied by the particles after filtration of 1 kg melt. This value is commonly adopted in the PoDFA analysis. The results revealed that the amount of inclusions increased significantly from 46×10^{-4} mm^2/kg to 494×10^{-4} mm^2/kg after 2 h of ultrasonic irradiation.

Fig. 8 presents a typical cross-sectional SEM image of a part of filter after the PoDFA analysis. Red-dotted lines separate areas inside filter pores from those corresponding the filter material between pores. Obviously, pores remain filled with solidified aluminum after the filtration treatment. In the case without UST, it is difficult to find inclusions in the pore, as shown in Fig. 8(b). However, a significant number of black rounded and polygonal inclusions are readily seen in the pore when an ingot after 2-hour UST was used for the PoDFA analysis. EDS analysis revealed that these inclusions are alumina particles. It is worthy of note that the size of inclusions agrees well with that of alumina particles collected from the melt surface (Fig. 6(b)). Thus, it is clear that UST results in entrainment of particles from the melt surface into the bulk, and these particles are fine alumina inclusions.

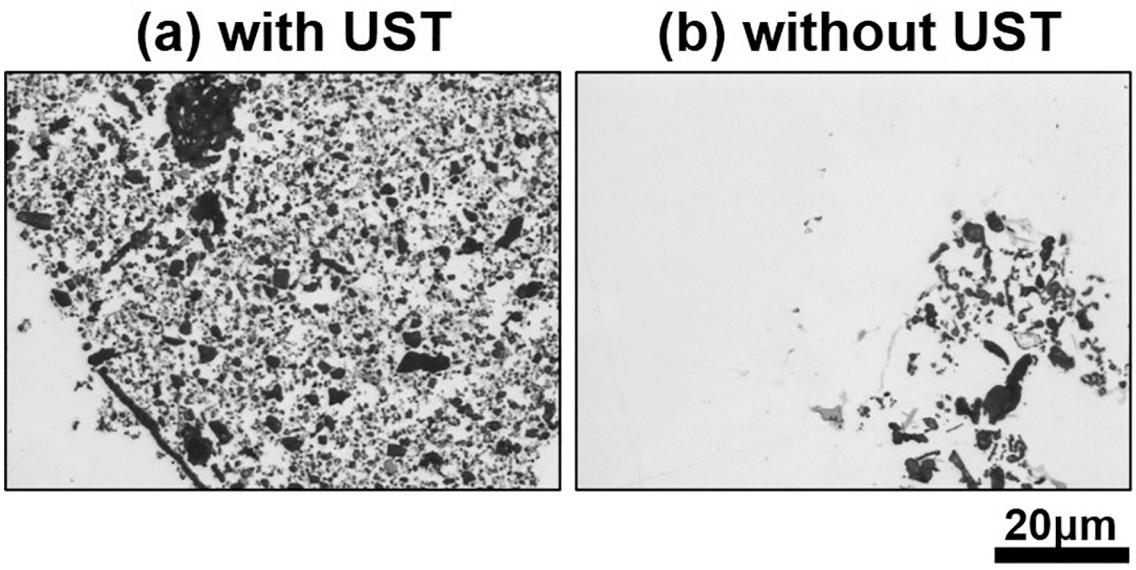

Fig. 7. The optical microscopy photos of samples after PoDFA analysis.

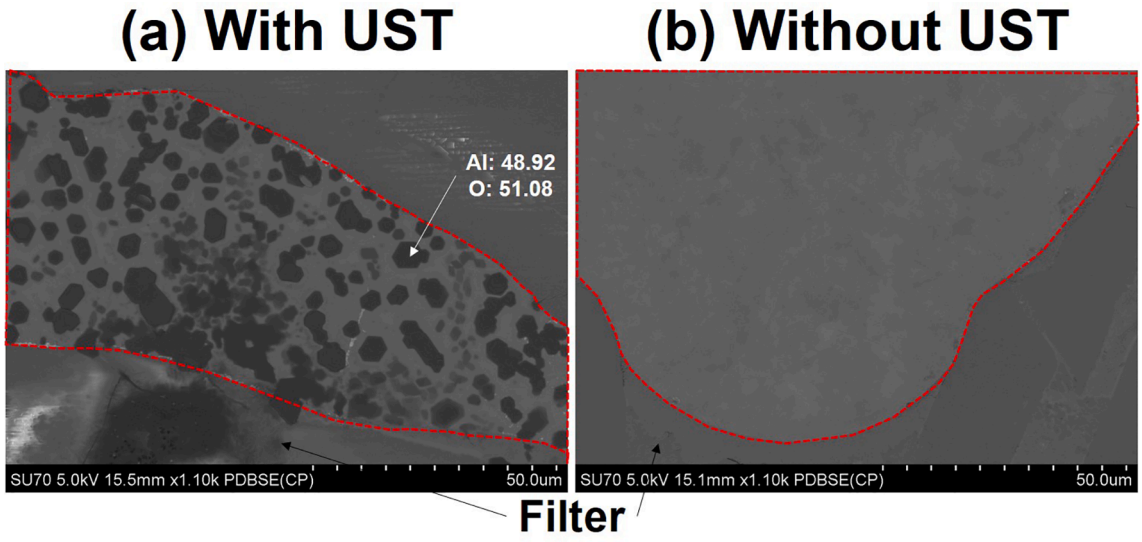

Fig. 8. SEM images of a part of filters after PoDFA tests: (a) sample after 2 h UST; (b) without UST.

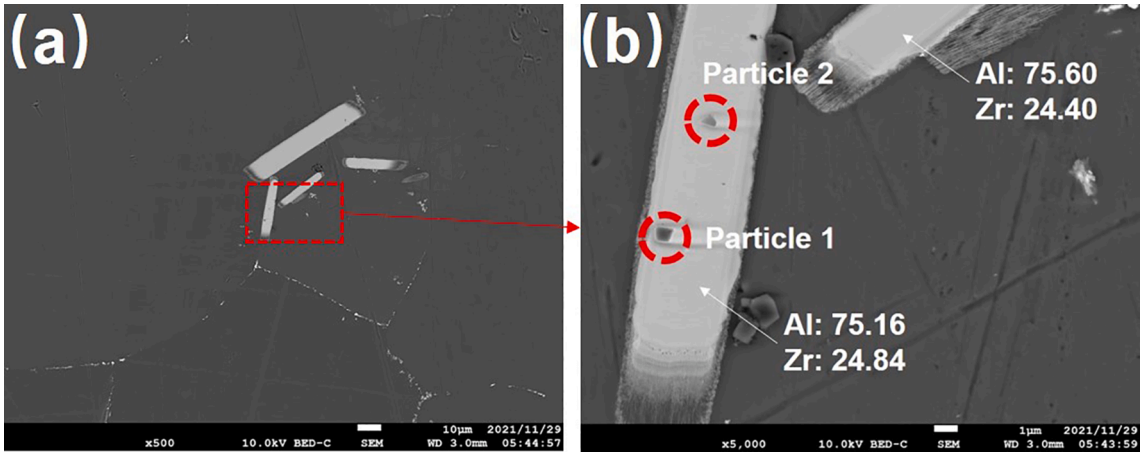

Fig. 9. Typical SEM microstructures of Al-0.4%Zr after 2 h UST.

3.3. Microstructural observation of Al-0.4%Zr alloy

Fig. 9(a) presents a typical SEM image of primary Al_3Zr particles after 2-hour UST. In order to see microstructural details, a part of image in the red-dotted square was enlarged and shown in Fig. 9(b). The particle composition was confirmed by the EDS point analysis showing that the atomic ratio of Al and Zr is around 3:1. Two dotted circles indicate the location of two smaller particles appear to be embedded in one of the above-mentioned Al_3Zr particles.

Fig. 10 reveals elemental mapping results for one Al_3Zr particle shown in Fig. 9. It is clearly seen that the particle is mainly composed of Al and Zr, but two fine particles embedded into the bulk of the large one contains oxygen. The bright field image and its mapping results in Fig. 11 also clearly indicate that the particle includes Al and Zr. More importantly, Fig. 11(b and d) reveals that the embedded particle consists of Al and O elements. As will be revealed in the next discussion section, these two particles are aluminum oxide particles.

3.4. TEM observation results

In order to identify the crystal structure of the particles and inclusions, TEM analysis was performed. The selected area for TEM investigation is marked by the upper red circle in the left side of Fig. 12. The specimen prepared using a focused ion beam (FIB) equipment for TEM observation is shown in Fig. 12(a). The TEM analysis indicates that the particle is composed of Al_3Zr phase, which has tetragonal DO_{23} structure (Fig. 12(b)), and the inclusion is composed of α-Al_2O_3 phase with a hexagonal structure (Fig. 12(c)). The Al_2O_3 inclusion is projected along the [010] zone axis, and the Al_3Zr particle is projected along the [0–31] zone axis. The high-resolution transmission electron microscopy (HRTEM) image in Fig. 12(d) shows the interface between the α-Al_2O_3 inclusion and Al_3Zr particle. It clearly seen that, despite the quite different crystal structure, Al_3Zr is tightly bound to the surface of Al_2O_3 inclusion suggesting that such inclusions can serve as nucleation sites for the primary Al_3Zr compounds. Similar results also have been reported by Wang et al. [36] and Jung et al. [37] The authors of the latter study obtained high-quality HR-TEM images revealing formation of a thin layer of γ-Al_2O_3 phase on the surface of alumina particles. This phase was shown to have a small (111) planar mismatch with (114) plane of $Al_3(Zr,Ti)$ used in their experiments. It is worth noting that some small amount of γ-Al_2O_3 phase was detected by XRD in powder collected from the melt surface in our experiments, as shown in Fig. 6(a).

4. Discussion

Thus, the above experimental results reveal that irradiation of high-intense ultrasound waves into molten aluminum promotes formation of oxide particles on the melt free surface and their entrainment from the surface into the melt bulk. These particles can serve as nucleation sites for crystallization of new phases, particularly intermetallic compounds. Below is a discussion on possible underlaying mechanisms and related phenomena.

4.1. Results of water model experiments

First, water model experiments were carried out to observe the entrainment of model particles into a water bath. Fig. 13 presents snapshots of video recording data showing the behavior of model particles on the free surface and their entrainment into the cavitation zone. Fig. 13(a) shows the initial situation, namely the profile of the free surface before starting the ultrasound irradiation. It is particularly remarkable that the free surface deviates from horizontal level revealing that the wetting angle is slightly lower than 90 degrees. After the ultrasound is turned on, the particles begin to move up the inclined surface of water towards the sonotrode as shown by arrows in Fig. 13(b), where they are entrained into downstream moving in parallel to the sonotrode wall and finally enter into the cavitation zone as can be seen from Fig. 13(c). Mechanisms and driving forces of particle motion will be discussed below. Some particles also can be entrained into water from the free surface during its oscillations. The red-dotted square in Fig. 13(e) shows a local deformation of the free surface after disturbing by ultrasound causing the free surface oscillations and particle entrainment. The frequency of the free surface oscillations is much lower compared to the frequency of ultrasound waves because the oscillations are caused mainly by large-scale turbulent eddies and acoustic streaming. This mechanism is probably similar to that observed by Komarov et al. [31]

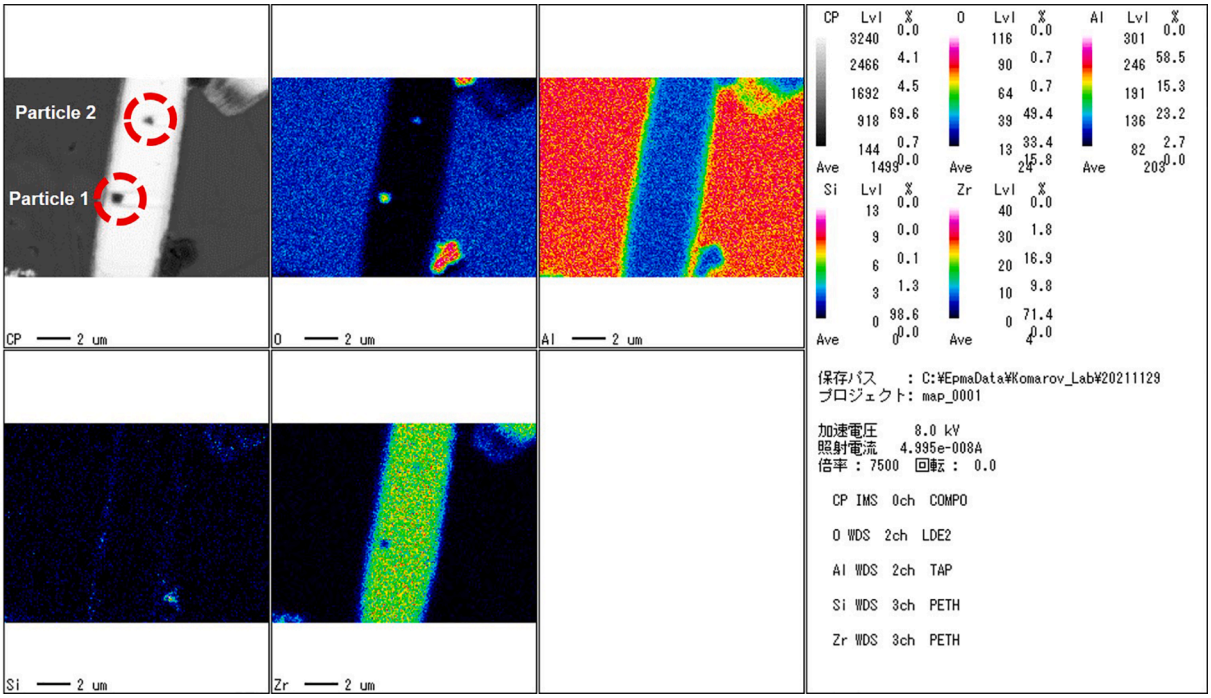

Fig. 10. Mapping results of elements for SEM microstructures.

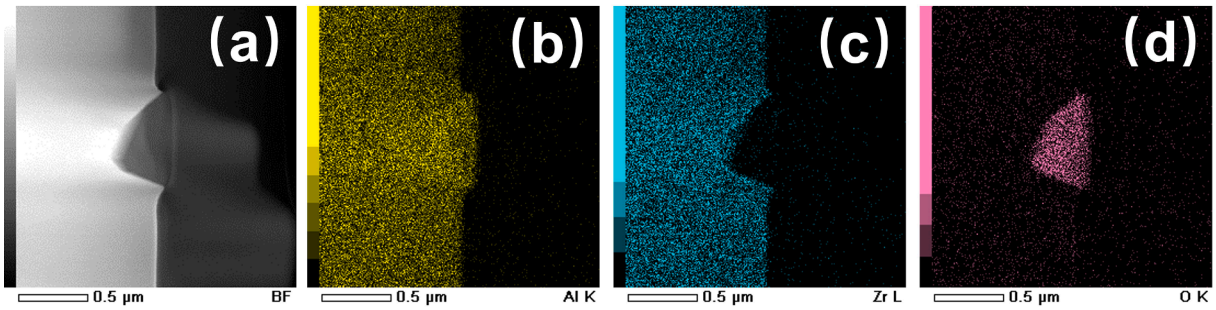

Fig. 11. (a) TEM bright field image in the vicinity of particle 2, and (b-d) EDS mapping results.

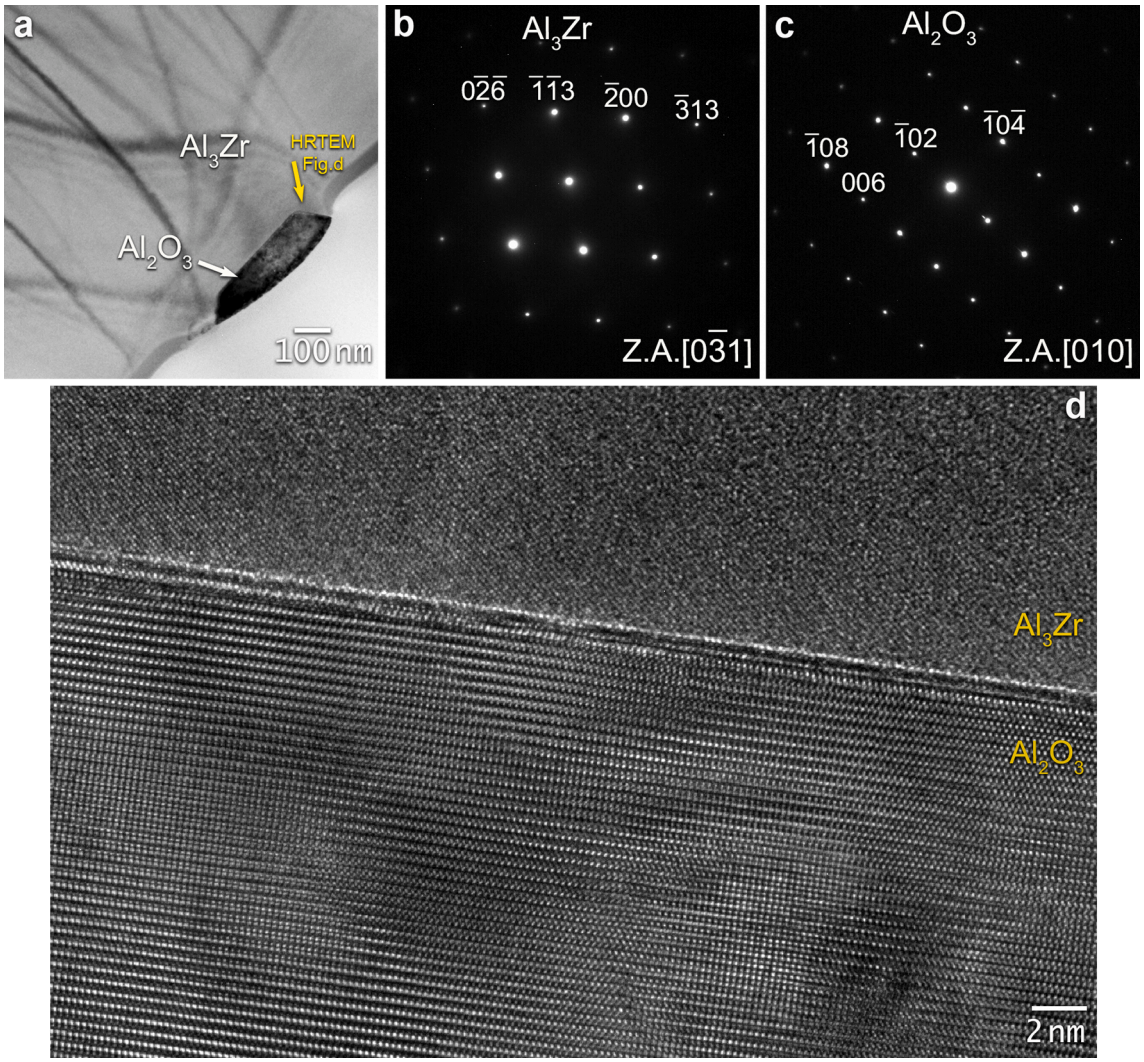

Fig. 12. TEM investigation of the particles and inclusions: (a) TEM image of a part of Al_3Zr particle; (b) the selected area electron diffraction (SAED) pattern of Al_3Zr particle; (c) SAED pattern of the Al_2O_3 inclusion; (d) HRTEM image of the interface between the Al_3Zr particle and the Al_2O_3 inclusion.

for a case when particles were entrained into water due to oscillating motion of vortex in a mechanically agitated water bath. Another interesting phenomenon is shown in Fig. 13(h and i). Some of the particles are seen to be aligned along a straight line indicated by the red arrow in Fig. 13(h). This arrangement of particles remains unchangeable for a while as seen from Fig. 13(i). Also, it is seen that other particles begin to line up in the same direction. Eventually, all particles were transferred into the cavitation zone. The line arrangement of particles is probably caused by the primary Bjerknes force acting on the particles in water in the presence of standing waves. Standing waves can form in the vessel due to reflection of ultrasound waves from the walls and free surface. This phenomenon has been well documented by Louisnard [38] for the case of fine bubble arrangement in a Bjerknes force field.

Thus, based on the results of water model experiments, it can be summarized that particle can be entrained from the free surface into the cavitation zone due to a number of mechanisms including downward acoustic flow, free surface oscillations and eddies near the sonotrode. One more factor influencing the entrainment phenomena is wettability

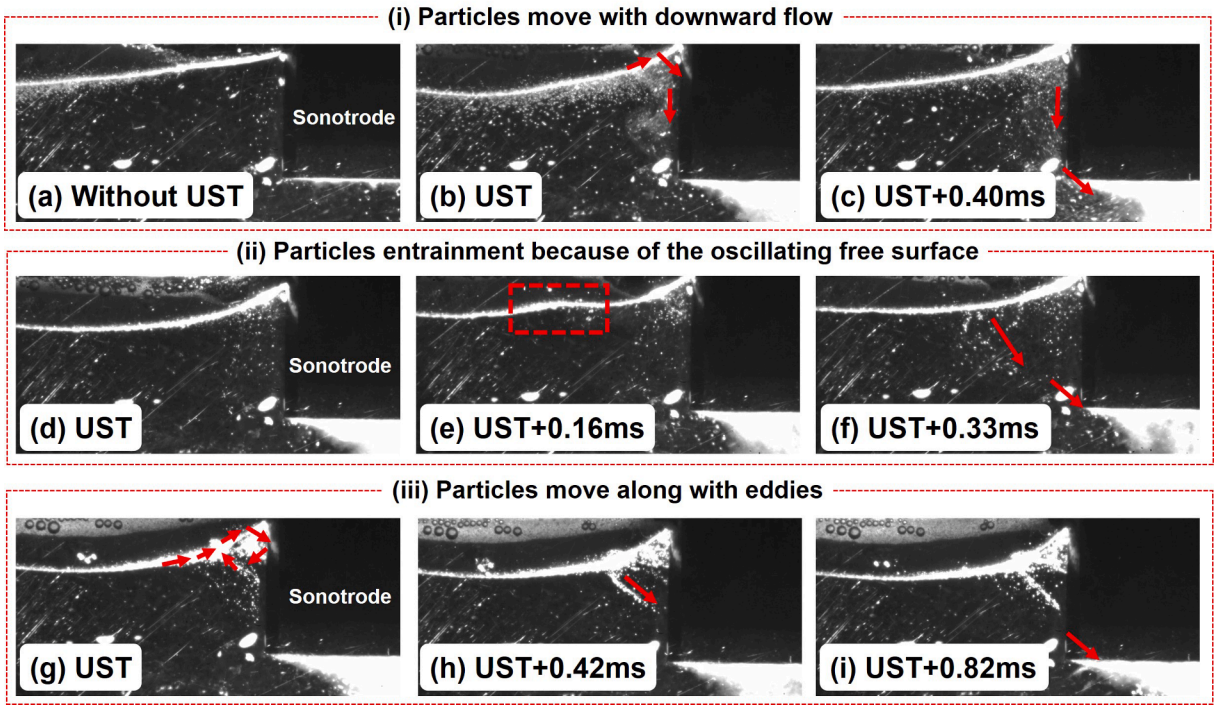

Fig. 13. Snapshots showing the particles penetration into water near the sonotrode: (i) particles move downward; (ii) particles are entrained due to oscillations of free surface; (iii) particles move along with eddies.

of particles by liquid. Obviously, the poorer the wettability is, the more difficult it is for particles to penetrate into liquid. As alumina is poorly wetted by molten aluminum, the penetration of alumina particles into melt is expected to occur to a lesser extent compared to the PMMA particle case.

4.2. Consideration on phenomena occurring at the free surface

As mentioned above a lot of alumina particles were discovered on the surface of pure Al melts after 2-hour UST. Accumulation of such particles was observed especially around the sonotrode. It is clear that aluminum melt is immediately oxidized to form a thin oxide layer when its surface is exposed to oxygen-containing atmosphere. The notable feature of this layer is a very small thickness and high melting temperature, more than 2000^{O}C. Therefore, alumina layer floats on the free surface of liquid aluminum as island-like films or conglomerates of particles which can be easily broken into smaller fragments or individual particles. Moreover, since the density of alumina is larger than molten alumina, the particles are retained on the surface only under the action of capillary forces. Also, it is obvious that Al oxidation at melt surface occurs not only due to reaction with atmospheric oxygen but also with the moisture. In this case, a reaction of Al with H_2O produces hydrogen and alumina. Hydrogen dissolves in the melt that can facilitate cavitation inception and make the cavitation zone wider. Although experimental investigations of cavitation zone present serious difficulties, some characteristics of cavitation zone can be predicted numerically. For example, Fang et al. [2] predicted distribution of cavitation bubble volume fraction, β and the boundary of cavitation zone. Both are presented in Fig. 14. It is worth noting that the cavitation zone shown by the solid white line, extends not only downward but sideward of the sonotrode wall.

It is reasonable to assume that some cavitation bubbles generated in such a cavitation zone can become stable and float up to the free surface covered by oxide films. The collapsing or bursting of these bubbles at the free surface can cause its local disturbance or even droplet formation. Besides, collapsing bubbles can generate micro-jets directed to the free

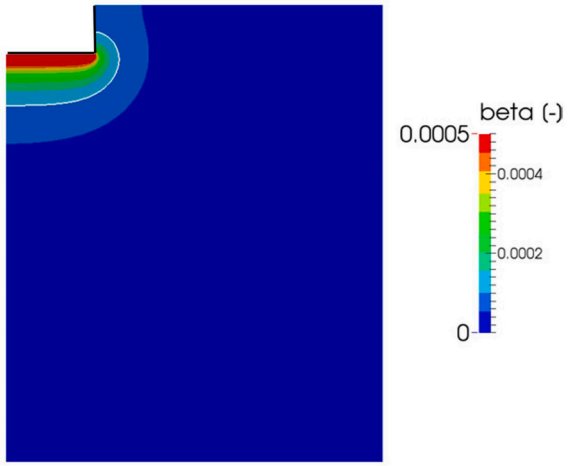

Fig. 14. Predicted distribution of bubble volume fraction and the boundary of cavitation zone (solid white lines) under the flat-tip sonotrode. [2].

surface. This phenomenon has been demonstrated by the experimental observations of Zhang et al. [39] revealing that cavitation bubbles induce micro-jet towards the free surface of water and such a micro-jet can cause formation of a hump on the free surface. Moreover, the effects of breaking or fragmentation of oxide films under the action of cavitation-induced micro-jet have been investigated by several researches [39–43]. For example, Zhang et al. [42] found that the high pressure generated by collapsing bubbles induces a shear force resulting in a shear deformation of oxide films. As a result, the films can be fragmented into tiny particles if the shear force is large enough or the cumulative shear deformation reaches the critical value. Obviously, the above-mentioned phenomena can cause not only a fragmentation of oxide films but an increase of aluminum oxidation due to a constant renewal of the surface in contact with oxidizing gas. Fig. 15 shows a schematic representation of the fragmentation process of oxide films by

the micro-jet. Fig. 15(a) shows a sonotrode immersed into Al melt during UST, and a part of the free surface in the red dotted circle is magnified and shown in Fig. 15(b and c).

Then, a part of particles, accumulated around the sonotrode, can be entrained into the bulk of melt as suggested by the above results of water model experiments. The main phenomenon, responsible for the particle entrainment, is the local acoustic streaming which occurs in the vicinity of sonotrode. Although the video recording equipment, used in the present study, did not allow direct observations of microscale turbulence and flows near the sonotrode surface, the entrainment of particles here is well documented by our water model experiments. Another evidence in support of this entrainment mechanism can be found in the above-mentioned study of Fang et al. [2] where the authors showed experimentally and numerically that liquid flows down from the free surface to the cavitation zone when ultrasound vibrations are introduced through a sonotrode with a flat tip. Thus, alumina particles can be entrained from the free surface of melt directly into the cavitation zone where they can be subjected to the further fragmentation and activation leading to improvement of their nucleation potency.

4.3. Possibility for controlling oxidation and entrainment of particles

The experimental results of the present study and the following discussion showed that the formation of alumina particles and their entrainment into molten aluminum occur in the vicinity of sonotrode. Therefore, both the particle formation and entrainment should be affected by conditions of ultrasound treatment. In the present study, the ultrasound treatment was performed for a long time using only 2 kg of aluminum melt. Clearly these conditions are favourable for the formation and entrainment of oxide particles. Long treatment time was required to collect a sufficient amount of oxide particles for their analysis. It is obvious that in actual practice, for example in ultrasonic casting, the treatment is performed under quite different conditions. Particularly, aluminum melt flows faster and passes through the near-sonotrode region for a much shorter time as compared to the treatment in a crucible. Furthermore, in practice the ultrasonic treatment time is usually much shorter. Therefore, the amount of oxide particles formed on the surface and entrained into melt can be expected to be much lower compared to our experiment case. Nevertheless, the following two factors, namely immersion depth of sonotrode in the melt and wettability between the sonotrode materials and aluminum melt are assumed to be of significant importance for controlling the formation and entrainment of oxide particles from the melt surface into its bulk. Below is a brief consideration on each of these factors.

The important role of sonotrode immersion depth can be seen from the above direct observations of particle motion in the vicinity of sonotrode in the water model experiments. In the present study, the sonotrode tip was submerged into the water bath to a small depth so that the cavitation zone was located close to the free surface. As a result, the cavitation bubbles and acoustic flows in the cavitation zone affected significantly the behavior of the free surface and particles floating on it. In the high temperature experiments, the sonotrode tip was submerged into the melt to a relatively small depth. This is assumed to be one of the reasons why such a great amount of alumina particles were observed on the melt surface and in the PoDFA samples. Immersion of the sonotrode deeper into the melt will increase the distance between the cavitation zone and the free surface that can suppress the formation and, more importantly, entrainment of oxide particles into the melt. Moreover, since ultrasound sonotrode is designed in such a way that the vibration amplitude is maximum at its tip, a deeper immersion of the sonotrode tip in the melt will provide a smaller vibration amplitude of sonotrode side wall at the location of the free surface. This may give an additional opportunity to control the particle formation and entrainment rates.

Finally, some comments should be made concerning the wettability between aluminum melt and sonotrode material. This factor may be important because the particle entrainment seems to occur in the immediate vicinity of sonotrode side wall where the liquid surface forms a meniscus and its curvature can be either positive or negative depending on the wettability and surface tension. The observations of the present study reveal that particles can be entrained into liquid even when the sonotrode surface is well-wetted by liquid and meniscus curvature is positive. This situation corresponds to that of ultrasound treatment using a metal sonotrode which is well-wetted by liquid aluminum. On the other hand, since non-reactive stable ceramics like silicon nitride are poorly wetted by liquid metals, the use of ceramic sonotrode can promote the particle entrainment due to a negative curvature of meniscus in this case. On the other hand, it is well known that ultrasonic vibration improves wettability of solids. This is supported, for example, by Sarasua et al. [44] who reported that ultrasonic vibrations result in reduction of the contact angle with no return. Therefore, we believe that the profile of aluminum melt surface near the sonotrode is not too different from what we observed in the water model experiments. Validity of this suggestion, however, should be carefully investigated in the follow-up studies.

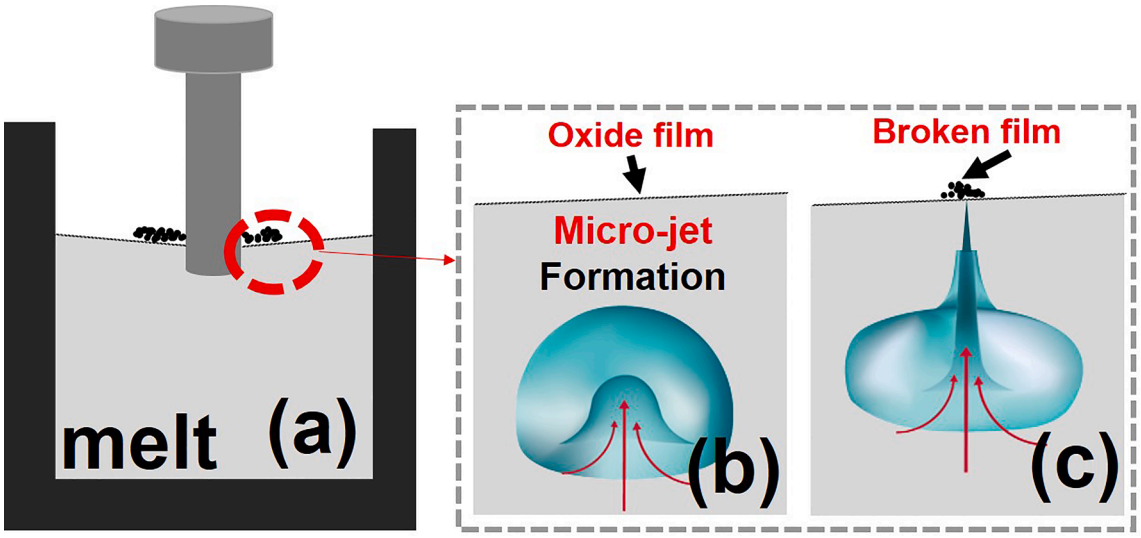

Fig. 15. A schematic representation of the fragmentation process of oxide films by the micro-jet: (a) a sonotrode immersed into Al melt during UST; (b) the cavitation bubble with micro-jet moves towards melt surface; (c) the micro-jet breaks oxide film.

5. Conclusions

In the present work, the ultrasound-disturbed free surface phenomena and their influence on ultrasonic treatment performance of aluminum alloys were investigated. The following phenomena were considered and investigated in the high temperature and water model experiments using ultrasound irradiation. (1) formation of oxide particles on the melt surface; (2) the behavior of the water free surface near the ultrasound sonotrode; (3) entrainment of particles from the free surface into water and aluminum melt; (4) nucleation of Al_3Zr intermetallic compounds on the surface of alumina particles. Based on the above results and discussion, the following conclusions can be drawn from this study.

1. Ultrasound irradiation greatly enhances the formation of alumina particles on the melt free surface around sonotrode. This is because cavitation-driven microstreaming, bubble burst and oscillations occurring near or on the free surface, disturb the surface enhancing its renewal. Besides, acoustic streaming, generated in the melt, causes the free surface to flow from the crucible sidewalls to sonotrode resulting in the accumulation of alumina particles near the sonotrode.
2. Another factor influencing the particle entrainment is oscillations of water free surface near the ultrasound sonotrode caused by large-scale turbulent eddies and acoustic streaming.
3. A part of particles can be entrained from the free surface into the cavitation zone and then transferred to the liquid bulk, as confirmed by PoDFA tests.
4. The primary Al_3Zr compound was found to be tightly bound to the surface of entrained alumina inclusion suggesting that the alumina particles can serve as nucleation sites for the Al_3Zr compounds.
5. Immersion depth of sonotrode into molten aluminum can be a very important operation variable to control the formation and entrainment of oxide particles from the free surface into the melt. This is because many free surface phenomena are strongly affected by cavitation and acoustic streaming occurring in the vicinity of the sonotrode tip.

Declaration of Competing Interest

The authors declare that they have no known competing financial interests or personal relationships that could have appeared to influence the work reported in this paper.

Data availability

No data was used for the research described in the article.

Acknowledgment

This work was partly sponsored by Chinese Scholarship Council (CSC).

Appendix A. Supplementary data

Supplementary data to this article can be found online at https://doi.org/10.1016/j.ultsonch.2022.106209.

References

[1] R.J. Lanyi, D.H. Lane, C.A. Forbes, H.E. Ricks, The Application of Ultrasonic Energy to Metal Processing, SAE Trans. 71 (1963) 520–562.
[2] Y. Fang, T. Yamamoto, S. Komarov, Cavitation and acoustic streaming generated by different sonotrode tips, Ultrason. Sonochem. 48 (2018) 79–87, https://doi.org/10.1016/j.ultsonch.2018.05.011.
[3] J. Berlan, T.J. Mason, Sonochemistry: from research laboratories to industrial plants, Ultrason. 30 (1992) 203–212, https://doi.org/10.1016/0041-624X(92)90078-Z.
[4] S. Komarov, K. Oda, Y. Ishiwata, N. Dezhkunov, Characterization of acoustic cavitation in water and molten aluminum alloy, Ultrason. Sonochem. 20 (2013) 754–761, https://doi.org/10.1016/j.ultsonch.2012.10.006.
[5] G.I. Eskin, Influence of cavitation treatment of melts on the processes of nucleation and growth of crystals during solidification of ingots and castings from light alloys, Ultrason. Sonochem. 1 (1994) S59–S63, https://doi.org/10.1016/1350-4177(94)90029-9.
[6] G.I. Eskin, Cavitation mechanism of ultrasonic melt degassing, S141, Ultrason. Sonochem. 2 (1995) S137, https://doi.org/10.1016/1350-4177(95)00020-7.
[7] G.I. Eskin, Broad prospects for commercial application of the ultrasonic (cavitation) melt treatment of light alloys, Ultrason. Sonochem. 8 (2001) 319–325, https://doi.org/10.1016/S1350-4177(00)00074-2.
[8] Z. Liu, R. Li, R. Jiang, L. Zhang, X. Li, Scalable Ultrasound-Assisted Casting of Ultra-large 2219 Al Alloy Ingots, Metall. Mater. Trans. A. 50 (2019) 1146–1152, https://doi.org/10.1007/s11661-018-5097-y.
[9] A.H. Idrisi, A.-H.-I. Mourad, Conventional stir casting versus ultrasonic assisted stir casting process: Mechanical and physical characteristics of AMCs, J. Alloys Compd. 805 (2019) 502–508, https://doi.org/10.1016/j.jallcom.2019.07.076.
[10] G. Chen, M. Yang, Y. Jin, H. Zhang, F. Han, Q. Chen, Z. Zhao, Ultrasonic assisted squeeze casting of a wrought aluminum alloy, J. Mater. Process. Technol. 266 (2019) 19–25, https://doi.org/10.1016/j.jmatprotec.2018.10.032.
[11] Y. Yang, J. Lan, X. Li, Study on bulk aluminum matrix nano-composite fabricated by ultrasonic dispersion of nano-sized SiC particles in molten aluminum alloy, Mater. Sci. Eng. A. 380 (2004) 378–383, https://doi.org/10.1016/j.msea.2004.03.073.
[12] G.I. Eskin, Ultrasonic Treatment of Light Alloy Melts, CRC Press, London (1998), https://doi.org/10.1201/9781498701792.
[13] O.V. Abramov, High-Intensity Ultrasonics: Theory and Industrial Applications, CRC Press, London (2020), https://doi.org/10.1201/9780203751954.
[14] D.G. Eskin, Physical Metallurgy of Direct Chill Casting of Aluminum Alloys, CRC Press, Boca Raton (2008), https://doi.org/10.1201/9781420062823.
[15] L. Zhang, D.G. Eskin, L. Katgerman, Influence of ultrasonic melt treatment on the formation of primary intermetallics and related grain refinement in aluminum alloys, J. Mater. Sci. 46 (2011) 5252–5259, https://doi.org/10.1007/s10853-011-5463-2.
[16] A. Priyadarshi, M. Khavari, T. Subroto, M. Conte, P. Prentice, K. Pericleous, D. Eskin, J. Durodola, I. Tzanakis, On the governing fragmentation mechanism of primary intermetallics by induced cavitation, Ultrason. Sonochem. 70 (2021), 105260, https://doi.org/10.1016/j.ultsonch.2020.105260.
[17] I. Tzanakis, G.S.B. Lebon, D.G. Eskin, K. Pericleous, Investigation of the factors influencing cavitation intensity during the ultrasonic treatment of molten aluminium, Mater. Des. 90 (2016) 979–983, https://doi.org/10.1016/j.matdes.2015.11.010.
[18] B. Wang, D. Tan, T.L. Lee, J.C. Khong, F. Wang, D. Eskin, T. Connolley, K. Fezzaa, J. Mi, Ultrafast synchrotron X-ray imaging studies of microstructure fragmentation in solidification under ultrasound, Acta Mater. 144 (2018) 505–515, https://doi.org/10.1016/j.actamat.2017.10.067.
[19] T.V. Atamanenko, D.G. Eskin, L. Zhang, L. Katgerman, Criteria of Grain Refinement Induced by Ultrasonic Melt Treatment of Aluminum Alloys Containing Zr and Ti, Metall. Mater. Trans. A. 41 (2010) 2056–2066, https://doi.org/10.1007/s11661-010-0232-4.
[20] S. Komarov, T. Yamamoto, Role of Acoustic Streaming in Formation of Unsteady Flow in Billet Sump during Ultrasonic DC Casting of Aluminum Alloys, Materials. 12 (2019) 3532, https://doi.org/10.3390/ma12213532.
[21] T. Yamamoto, S.V. Komarov, Influence of ultrasound irradiation on transient solidification characteristics in DC casting process: Numerical simulation and experimental verification, J. Mater. Process. Technol. 294 (2021), 117116, https://doi.org/10.1016/j.jmatprotec.2021.117116.
[22] S. Komarov, Y. Ishiwata, Y. Takeda, Ultrasonic Assisted Reduction of Hot-Tearing During High-Speed DC Casting of 6000 Series Aluminum Alloys, in: A.P. Ratvik (Ed.), Light Metals 2017, Springer International Publishing, Cham, 2017: pp. 989-994. https://doi.org/10.1007/978-3-319-51541-0_119.
[23] G.I. Eskin, D.G. Eskin, Production of natural and synthesized aluminum-based composite materials with the aid of ultrasonic (cavitation) treatment of the melt, Ultrason. Sonochem. 10 (2003) 297–301, https://doi.org/10.1016/S1350-4177(02)00158-X.
[24] S. Komarov, Y. Ishiwata, I. Mikhailov, Industrial Application of Ultrasonic Vibrations to Improve the Structure of Al-Si Hypereutectic Alloys: Potential and Limitations, Metall. Mater. Trans. A. 46 (2015) 2876–2883, https://doi.org/10.1007/s11661-015-2829-0.
[25] S. Komarov, Y. Ishiwata, K. Oda, Refinement of Primary Silicon in Casting Aluminum Alloys via Application of Ultrasonic Vibrations to DC process, in: 12th International Conference on Aluminium Alloys, Yokohama, Japan, 2010: pp. 652-657.
[26] V.M. Sreekumar, N. Hari Babu, D.G. Eskin, Prospects of In-Situ α-Al2O3 as an Inoculant in Aluminum: A Feasibility Study, J. of Materi Eng and Perform. 26 (2017) 4166–4176, https://doi.org/10.1007/s11665-017-2853-x.
[27] H.-T. Li, Y. Wang, Z. Fan, Mechanisms of enhanced heterogeneous nucleation during solidification in binary Al–Mg alloys, Acta Mater. 60 (2012) 1528–1537, https://doi.org/10.1016/j.actamat.2011.11.044.
[28] Z. Que, Y. Wang, C.L. Mendis, Heterogeneous nucleation of α-Al on naturally formed MgAl2O4 particles during solidification of Al–Mg–Si–Fe–Mn alloys, Materialia. 14 (2020), 100900, https://doi.org/10.1016/j.mtla.2020.100900.

[29] K. Kim, The Effect of Melt Conditioning on Segregation of Solute Elements and Nucleation of Aluminum Grains in a Twin Roll Cast Aluminum Alloy, Metall. Mater. Trans. A. 45 (2014) 4538–4548, https://doi.org/10.1007/s11661-014-2414-y.
[30] J. Liu, Q. Wang, Y. Qi, Atomistic simulation of the formation and fracture of oxide bifilms in cast aluminum, Acta Mater. 164 (2019) 673–682, https://doi.org/10.1016/j.actamat.2018.11.008.
[31] S. Komarov, T. Yamamoto, H. Arai, Incorporation of Powder Particles into an Impeller-Stirred Liquid Bath through Vortex Formation, Materials. 14 (2021) 2710, https://doi.org/10.3390/ma14112710.
[32] Q. Kang, X. Feng, C. Yang, J. Wang, DEM-VOF simulations on the drawdown mechanisms of floating particles at free surface in turbulent stirred tanks, Chem. Eng. J. 431 (2022), 133275, https://doi.org/10.1016/j.cej.2021.133275.
[33] J. Sun, T. Yamamoto, S. Komarov, Behavior of Al-Zr intermetallic compound particles under high-amplitude ultrasound irradiation into molten aluminum, J. Alloys Compd. 912 (2022), 165128, https://doi.org/10.1016/j.jallcom.2022.165128.
[34] S. Komarov, T. Yamamoto, Development and Application of Large-Sized Sonotrode Systems for Ultrasonic Treatment of Molten Aluminum Alloys, in: C. Chesonis (Ed.), Light Metals 2019, Springer International Publishing, Cham, 2019, pp. 1597–1604, https://doi.org/10.1007/978-3-030-05864-7_202.
[35] C. Stanică, P. Moldovan, Aluminum melt cleanliness performance evaluation using PoDFA (porous disk filtration apparatus) technology, UPB Scientific Bulletin, Series B: Chemistry and Materials Science. 71 (2009).
[36] D. Wang, Q. Liu, Influence of aggregation/dispersion state of hydrophilic particles on their entrainment in fine mineral particle flotation, Miner. Eng. 166 (2021), 106835, https://doi.org/10.1016/j.mineng.2021.106835.
[37] J.-G. Jung, Y.-H. Cho, S.-D. Kim, S.-B. Kim, S.-H. Lee, K. Song, K. Euh, J.-M. Lee, Mechanism of ultrasound-induced microstructure modification in Al-Zr alloys, Acta Mater. 199 (2020) 73–84, https://doi.org/10.1016/j.actamat.2020.08.025.
[38] O. Louisnard, A simple model of ultrasound propagation in a cavitating liquid. Part II: Primary Bjerknes force and bubble structures, Ultrason. Sonochem. 19 (2012) 66–76, https://doi.org/10.1016/j.ultsonch.2011.06.008.
[39] A.M. Zhang, P. Cui, J. Cui, Q.X. Wang, Experimental study on bubble dynamics subject to buoyancy, J. Fluid Mech. 776 (2015) 137–160, https://doi.org/10.1017/jfm.2015.323.
[40] Y.-J. Chen, W.-N. Hsu, J.-R. Shih, The Effect of Ultrasonic Treatment on Microstructural and Mechanical Properties of Cast Magnesium Alloys, Mater. Trans. 50 (2009) 401–408, https://doi.org/10.2320/matertrans.MER2008273.
[41] Y.-J. Chen, L.-W. Huang, T.-S. Shih, Diagnosis of Oxide Films by Cavitation Micro-Jet Impact, Mater. Trans. 44 (2003) 327–335, https://doi.org/10.2320/matertrans.44.327.
[42] Y. Zhang, R. Li, X. Li, Y. Yang, P. Chen, F. Dong, R. Jiang, Possible Effects and Mechanisms of Ultrasonic Cavitation on Oxide Inclusions during Direct-Chill Casting of an Al Alloy, Metals. 8 (2018) 814, https://doi.org/10.3390/met8100814.
[43] N.S.M. Yusof, B. Babgi, Y. Alghamdi, M. Aksu, J. Madhavan, M. Ashokkumar, Physical and chemical effects of acoustic cavitation in selected ultrasonic cleaning applications, Ultrason. Sonochem. 29 (2016) 568–576, https://doi.org/10.1016/j.ultsonch.2015.06.013.
[44] J.A. Sarasua, L.R. Rubio, E. Aranzabe, J.L.V. Vilela, Energetic study of ultrasonic wettability enhancement, Ultrason. Sonochem. 79 (2021), 105768, https://doi.org/10.1016/j.ultsonch.2021.105768.